Monazite transformation into Ce- and La-containing oxalates by Aspergillus niger

Kang, Xia; Csetenyi, Laszlo; Gadd, Geoffrey Michael

Published in:
Environmental Microbiology

DOI:
10.1111/1462-2920.14964

Publication date:
2020

Document Version
Publisher's PDF, also known as Version of record

environmental microbiology

Environmental Microbiology (2020) **00**(00), 00–00 doi:10.1111/1462-2920.14964

Monazite transformation into Ce- and La-containing oxalates by *Aspergillus niger*

Xia Kang,[1] Laszlo Csetenyi[2] and Geoffrey Michael Gadd [1,3]*

[1]*Geomicrobiology Group, School of Life Sciences, University of Dundee, Dundee, DD1 5EH, Scotland, UK.*

[2]*Concrete Technology Group, Department of Civil Engineering, University of Dundee, Dundee, DD1 4HN, Scotland, UK.*

[3]*State Key Laboratory of Heavy Oil Processing, Beijing Key Laboratory of Oil and Gas Pollution Control, College of Chemical Engineering and Environment, China University of Petroleum, 18 Fuxue Road, Changping District, Beijing, 102249, China.*

Summary

Monazite is a naturally occurring lanthanide (Ln) phosphate mineral [$Ln_x(PO_4)_y$] and is the main industrial source of the rare earth elements (REE), cerium and lanthanum. Endeavours to ensure the security of supply of elements critical to modern technologies view bioprocessing as a promising alternative or adjunct to new methods of element recovery. However, relatively little is known about microbial interactions with REE. Fungi are important geoactive agents in the terrestrial environment and well known for properties of mineral transformations, particularly phosphate solubilization. Accordingly, this research examined the capability of a ubiquitous geoactive soil fungus, *Aspergillus niger*, to affect the mobility of REE in monazite and identify possible mechanisms for biorecovery. It was found that *A. niger* could grow in the presence of monazite and mediated the formation of secondary Ce and La-containing biominerals with distinct morphologies including thin sheets, orthorhombic tablets, acicular needles, and rosette aggregates which were identified as cerium oxalate decahydrate ($Ce_2(C_2O_4)_3{\cdot}10H_2O$) and lanthanum oxalate decahydrate ($La_2(C_2O_4)_3{\cdot}10H_2O$). In order to identify a means for biorecovery of REE via oxalate precipitation the bioleaching and bioprecipitation potential of biomass-free spent culture supernatants was investigated. Although such indirect bioleaching of REE was low from the monazite with maximal lanthanide release reaching >40 mg L^{-1}, leached REE were efficiently precipitated as Ce and La oxalates of high purity, and did not contain Nd, Pr and Ba, present in the original monazite. Geochemical modelling of the speciation of oxalates and phosphates in the reaction system confirmed that pure Ln oxalates can be formed under a wide range of chemical conditions. These findings provide fundamental knowledge about the interactions with and biotransformation of REE present in a natural mineral resource and indicate the potential of oxalate bioprecipitation as a means for efficient biorecovery of REE from solution.

Introduction

Monazite is a group of monoclinic phosphates mainly comprising rare earth elements (REE), e.g. cerium, lanthanum and neodymium, and has long been regarded as a strategic resource coveted by the World's great powers such as China, Europe, USA and Japan because of its critical involvement in high-technology sectors including consumer electronics, clean energy, hybrid electric vehicles and weapons systems (Humphries, 2012; Massari and Ruberti, 2013; Goodenough *et al*., 2016). More than 70% of the global supply of monazite is restricted to only a few rich mine deposits and the content of Ce in commercial monazite concentrate ranges from 42.7% (Guangdong, China) to 51.0% (Mount Weld, Australia) while that of La ranges from 17.5% (Green Cove Springs, USA) to 26.0% (Mount Weld, Australia) of the total REE present (Massari and Ruberti, 2013; Moss *et al*., 2013; Kumari *et al*., 2015).

Monazite concentrate is usually separated from monazite-bearing ores by crushing and flotation or through gravity and electrostatic separation (Moustafa and Abdelfattah, 2010; Khanchi *et al*., 2014; Chelgani *et al*., 2015). Since monazite occurs as lanthanide-phosphate minerals of general formula $Ln_x(PO_4)_y$, it was thought to have limited interactions in terrestrial environments due to its high chemical and thermal stability and extremely low solubility: solubility products for $CePO_4$ and $LaPO_4$ are $K_{sp} = 1 \times 10^{-23}$ and $K_{sp} = 3.7 \times 10^{-23}$ respectively (Zhenghua *et al*., 2001). Traditional methods

Received 20 December, 2019; revised 19 February, 2020; accepted 26 February, 2020. *For correspondence. E-mail g.m.gadd@dundee.ac.uk; Tel: +44 1382 384767.

for recovering REE from concentrate include direct leaching using strong acids, e.g. sulphuric, nitric, and hydrochloric acid or strong alkalis, e.g. sodium hydroxide (Panda *et al*., 2014; Kumari *et al*., 2015):

$$LnPO_{4(s)} + 3H^{+}{}_{(aq)} \rightarrow Ln^{3+}{}_{(aq)} + H_3PO_{4(aq)} \quad (1)$$

$$LnPO_{4(s)} + 3OH^{-}{}_{(aq)} \rightarrow Ln(OH)_{3(s)} + PO_4{}^{3-}{}_{(aq)} \quad (2)$$

The resulting products can be recovered using precipitation agents before they are finally thermally decomposed to oxides. Although traditional leaching approaches are efficient, the use of strong acids and alkalis can be environmentally hazardous. In recent years, sustainable bioprocessing alternatives have been proposed, most focusing on element bioleaching and biorecovery from REE-bearing minerals by applying microbial systems (Zhuang *et al*., 2015; Liang and Gadd, 2017). Such biohydrometallurgical approaches are based on the biological mobilization of REE from solid-state materials including ore concentrate, electronic waste, mining residues and other metal-containing substrates with most attention being devoted to bacterial systems because of their well-known efficiency and established exploitation in bioleaching of metals such as copper and cobalt (Rawlings *et al*., 2003; Barmettler *et al*., 2016; Ng *et al*., 2016). However, in some previous research, citric acid-overproducing *Aspergillus ficuum* was used to treat Egyptian monazite (Th-U) which resulted in high bioleaching efficiencies of 75.4% and 63.8% under pulp densities of 0.6% and 1.2% (w/v) respectively (Hassanien *et al*., 2013). Other work showed that biomass-free spent medium of *A. terreus* ML3-1 and a *Paecilomyces* sp. WE3-F were 1.7–3.8 times more efficient in leaching REE from monazite than the amounts recovered using abiotic controls (Brisson *et al*., 2016). It has been established that one of the most important mechanisms underlying fungal bioleaching is the excretion of low-molecular-weight organic acids (Deng *et al*., 2013; Reed *et al*., 2016).

Aspergillus niger is a ubiquitous environmental fungus known for many industrial applications including citric acid production (Jernejc *et al*., 1982). It also possesses significant biogeochemical properties that enable interactions with metals and minerals such as mineral dissolution and biologically–induced mineralization (BIM), both of which can be mediated by the extracellular excretion of organic acids (Gadd, 2010; Li *et al*., 2014; Yang *et al*., 2019a; Yang *et al*., 2019b). *Aspergillus niger* is an efficient producer of oxalic acid ($H_2C_2O_4$), which can play a critical role in the BIM process for the bioprecipitation of a number of metals from soluble and insoluble sources (Gadd *et al*., 2014). For example, *A. niger* can transform $Co_3(PO_4)_2$, $Zn_3(PO_4)_2$ and ZnO into corresponding insoluble metal oxalates via an intermediate solubilization phase (Sayer and Gadd, 1997). Other studies have shown that *A. niger* was able to solubilize and precipitate calcium from natural gypsum ($CaSO_4{\cdot}2H_2O$) as calcium oxalate (Gharieb *et al*., 1998). This fungal species is also capable of transforming more complex minerals such as malachite ($Cu_2(CO_3)(OH)_2$) into copper oxalate (Fomina *et al*., 2017). Another example showed that lead oxalate was precipitated by *A. niger* in Pb^{2+}-containing media when supplemented with organic phosphate as the P source (Liang *et al*., 2016). *Aspergillus niger* has been shown to be an effective agent for the recovery of lanthanides including Ce and La from solution (Zhuang *et al*., 2015). Kang *et al.* (2019) described a novel method of recovering lanthanum as lanthanum oxalate from aqueous solution using biomass-free culture supernatants after the growth of *A. niger*. In general, it is assumed that biogenic oxalate can interact with phosphate through the following mechanisms (Chi and Xu, 1999; Furrow *et al*., 2012):

$$H_2C_2O_{4(aq)} \rightleftharpoons H^{+}{}_{(aq)} + HC_2O_4{}^{-}{}_{(aq)} \quad K_{a1} = 5.90 \times 10^{-2} \quad (3)$$

$$HC_2O_4{}^{-}{}_{(aq)} \rightleftharpoons H^{+}{}_{(aq)} + C_2O_4{}^{2-}{}_{(aq)} \quad K_{a2} = 6.40 \times 10^{-5} \quad (4)$$

$$LnPO_{4(s)} \rightleftharpoons Ln^{3+}{}_{(aq)} + PO_4{}^{3-}{}_{(aq)} \quad K_{sp} = \sim 10^{-23} \quad (5)$$

$$2Ln^{3+}{}_{(aq)} + 3C_2O_4{}^{2-}{}_{(aq)} \rightleftharpoons Ln_2(C_2O_4)_{3(s)} \quad K_{eq} = \sim 10^{26} \quad (6)$$

Since the solubility product of lanthanide oxalate, K_{sp} $[Ln_2(C_2O_4)_3] = [Ln^{3+}][C_2O_4{}^{2-}] = \sim 10^{-26}$, is lower than that of $LnPO_4$ ($\sim 10^{-23}$), speciation of oxalate-containing secondary minerals during interaction of monazite-containing rare earth phosphates in an acidic fungal-induced environment could be a profitable approach for biorecovery and worthy of examination. Bioprocessing is currently viewed as a promising alternative or adjunct to new methods of element recovery to ensure the security of supply of valuable strategic elements but little is known about microbial interactions with REE. Since fungi are important geoactive agents in the terrestrial environment and well known for properties of mineral transformations, particularly phosphate solubilization, the objective of this research was to examine the capability of a ubiquitous geoactive soil fungus, *Aspergillus niger*, to affect the mobility of REE in monazite with a view to identifying possible mechanisms for biorecovery. The results contribute a new understanding of the interactions between geoactive fungi and REE-containing minerals with potential practical applications.

Results

Fungal growth on solid medium

It was found that the presence of monazite had an influence on the growth of *A. niger* over 2 weeks of incubation. The surface pH of the monazite-containing agar

plates ranged from pH 3.55 to 3.74, which was significantly higher ($P < 0.05$) than the monazite-free control, which was at pH 2.75 (Fig. 1A). Fungal biomass yield, however, showed a significant declining trend as the monazite concentration increased. In particular, plates with 0.5% and 1.0% added monazite yielded 30% and 39% less biomass respectively, compared with the untreated controls (Fig. 1B). In plates supplemented with 0.5% monazite, a significant ($P < 0.05$) rise of surface pH was observed after 2 weeks of incubation compared with the first week (pH 2.94). The surface pH was maintained around pH 4.3 for the following 3 weeks (Fig. 1C). The biomass yield on these plates showed a general increasing trend as the incubation time increased (Fig. 1D).

REE concentrations and pH changes in liquid media

Changes in total REE concentration and pH were recorded over the course of a 5-week reaction of 2% monazite with spent Modified Czapek-Dox (MCD) culture medium (Fig. 2). The amount of REE leached out was low (7.3 mg L^{-1}) over the first week but dramatically increased to 39.9 mg L^{-1} by the second week and reached the maximal value of 43.1 mg L^{-1} by the third week. However, the fourth and fifth weeks saw a significant reduction of 53.5% and 58.7% respectively, compared with the maximum value. The overall pH followed a slow upward trend over the whole length of the liquid interaction, reaching a maximum (pH 2.92) by the fourth

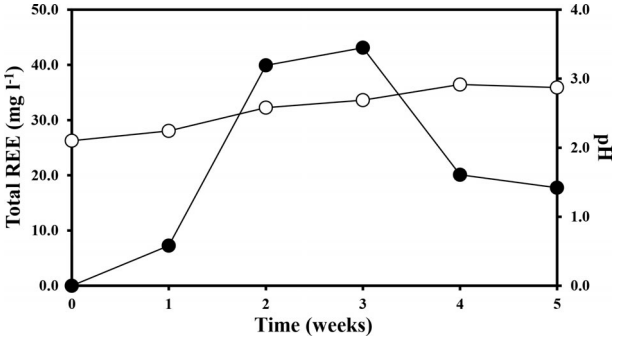

Fig. 2. Total rare earth concentration and pH of biomass-free spent liquid MCD culture medium supplemented with 2% (w/v) monazite and maintained on a roller mixer at 25°C in the dark. MCD medium was inoculated with *A. niger* and incubated at 25°C in the dark for 14 days prior to harvesting of the biomass-free culture supernatant. —●—, total REE; —○—, pH. Data are averages of at least three replicates: error bars representing the standard error of the mean are smaller than the symbol dimensions.

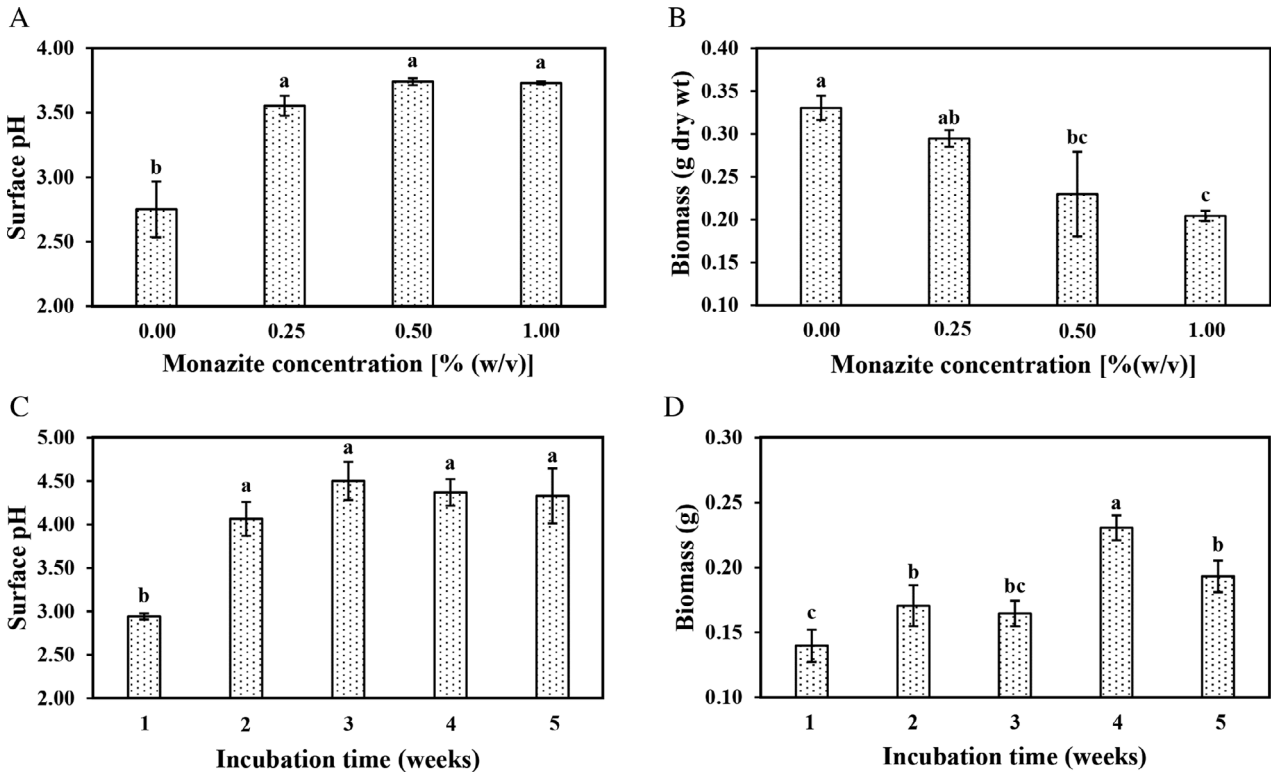

Fig. 1. (A) Surface pH of agar and (B) biomass yield of *A. niger* after 2 weeks incubation at 25°C in the dark on MCD plates containing different concentrations of monazite. Changes of (C) surface pH and (D) biomass yield of *A. niger* following 5 weeks growth on MCD plates supplemented with 0.5% (w/v) monazite under the same conditions. Data are averages of at least three replicates and error bars show the standard error of the mean. Different lowercase letters between treatments indicate differences are significant at $P < 0.05$ based on Tukey's test.

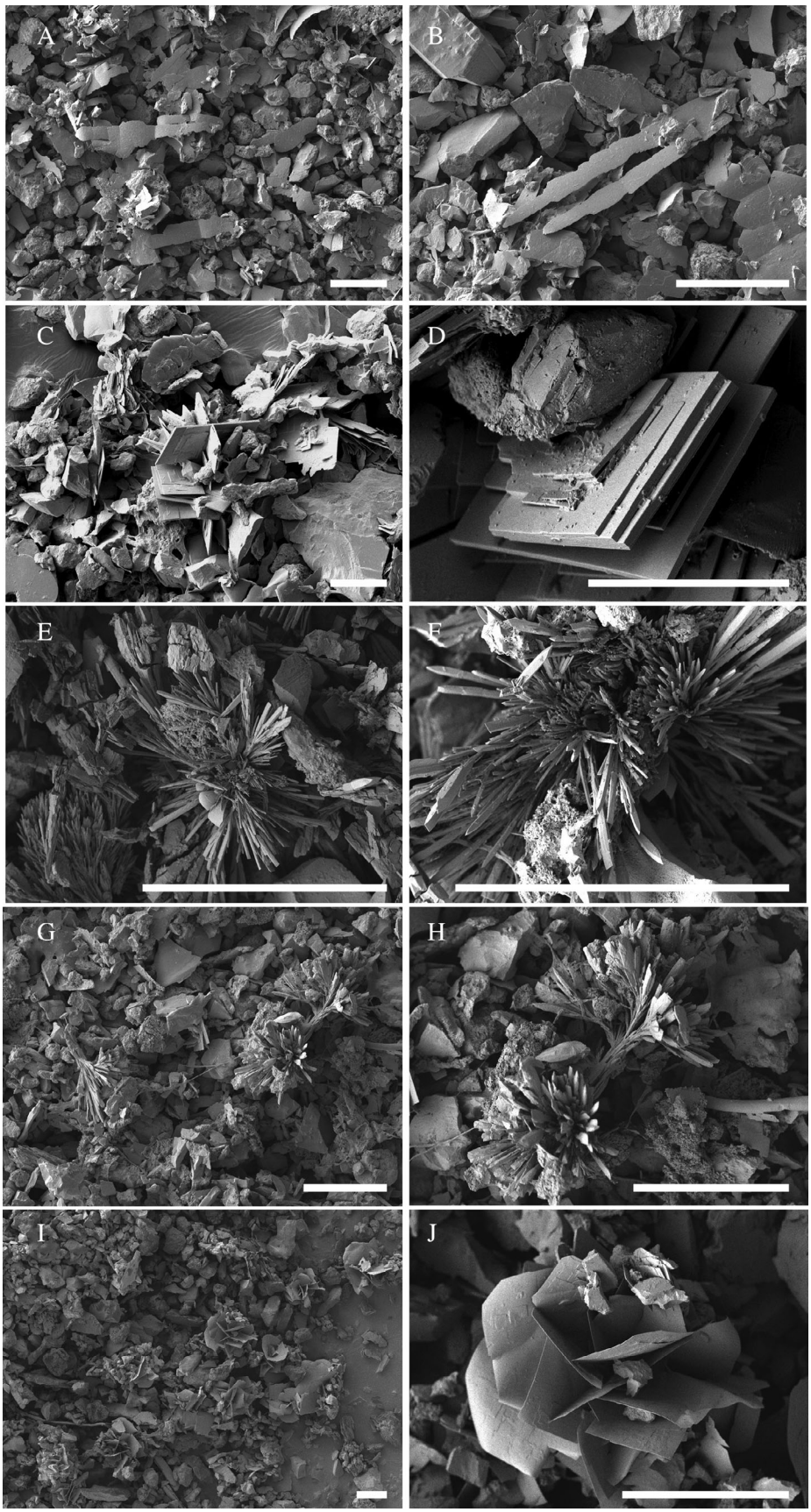

Fig. 3. Scanning electron microscopy (SEM) of the secondary biominerals extracted from solid MCD media containing 0.5% (w/v) monazite after (A and B) 1, (C and D) 2, (E and F) 3, (G and H) 4, and (I and J) 5 weeks growth of *A. niger* at 25°C in the dark. Scale bars: (A, B, E–J) are 100 μm, (C) 50 μm and (D) 20 μm. Typical images are shown from many similar examinations.

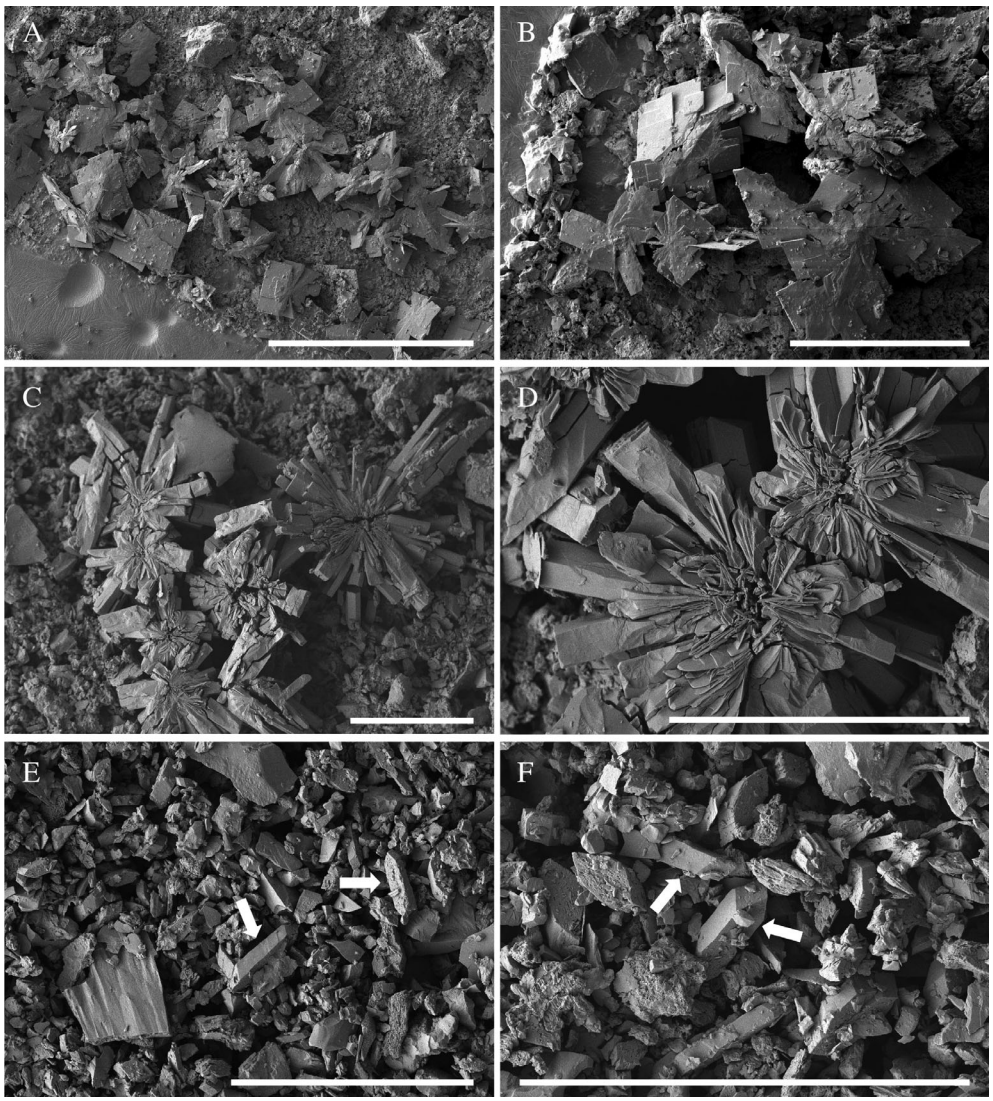

Fig. 4. Scanning electron microscopy (SEM) of the secondary biominerals produced as a result of the reaction of 1%(w/v) monazite with biomass-free *A. niger*-spent liquid MCD medium for (A and B) 1, (C and D) 2 and (E and F) 5 weeks at 25°C in the dark. Scale bars: (A) 500 μm, (B) 200 μm and (C–F) 50 μm. Typical images are shown from several similar examinations.

week and this only slightly decreased in the last week of incubation.

SEM and EDXA of produced biominerals

After growth of *A. niger* on 0.5% MCD agar plates, the formation of secondary biominerals was observed using scanning electron microscopy (SEM), which revealed distinctive morphological features varying in shapes and sizes at different incubation times. Large single crystals measuring ~200 μm in length and of a thin lamellar structure were found to be the only morphotype of the secondary minerals after incubation of *A. niger* for 1 week (Fig. 3A and B). After 2 weeks of incubation, the predominant biominerals were square-shaped tabular plates that grew out of the grains of the substrate (Fig. 3C and D). These structures ranged from ~20 to 60 μm in width but were much thicker than those crystals produced in the first week samples. Well-formed acicular structures consisting of radiating needles were discovered after 3 weeks of incubation. These needle-like crystals had disphenoid tips and formed large clusters measuring ~100 μm across (Fig. 3E and F). Acicular crystals were still the major structure at the fourth week of incubation. However, the needles tended to become broader and shorter and the clusters appeared to be in a less organized fashion (Fig. 3G and H). After 5 weeks of incubation, there was a complete change in the crystal

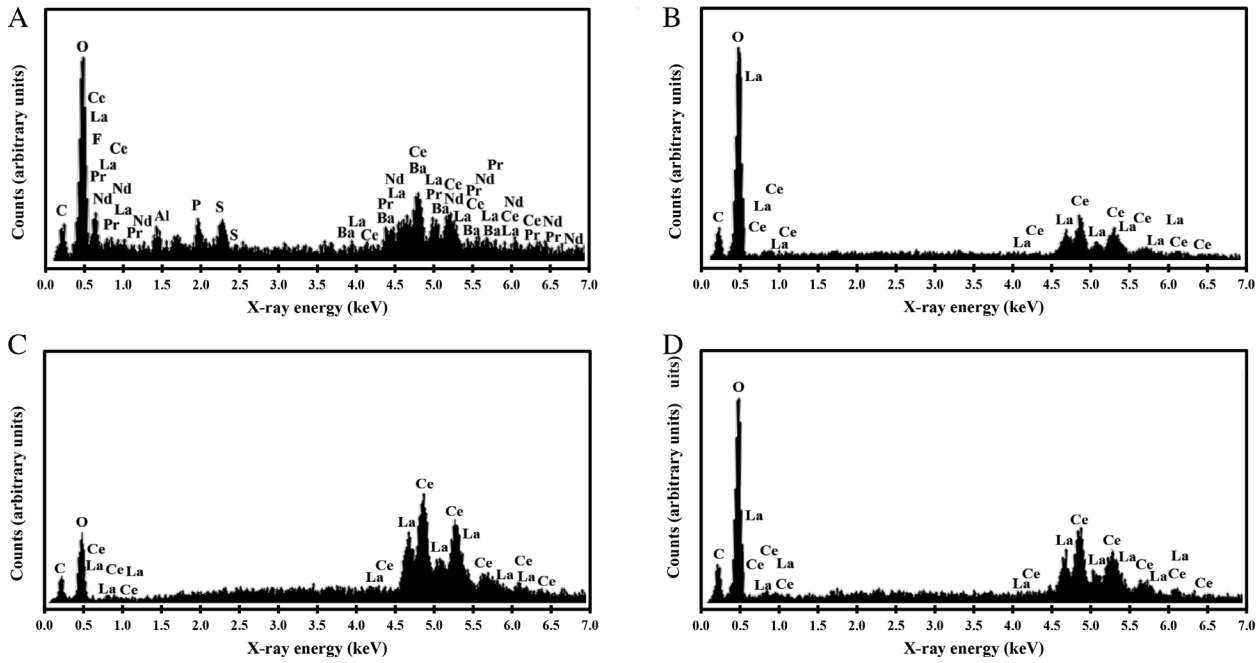

Fig. 5. Energy-dispersive X-ray analysis (EDXA) of (A) the original Gakara monazite and of the secondary biominerals extracted from solid MCD media containing 0.5% (w/v) monazite after (B) 1 and 2, (C) 3 and 4 and (D) 5 weeks growth of *A. niger* at 25°C in the dark. Typical spectra are shown from several similar determinations.

habit of the biominerals, which were all of a rosette structure composed of thin layers and forming large aggregates (Fig. 3I and J). However, morphological changes for the samples that were mixed with the biomass-free spent MCD liquid culture medium were not so varied and secondary minerals with distinct features were observed only in the first and second weeks. Diamond-shaped tabular structures were most abundant in 1-week samples and these formed large aggregates (~200 μm) by stacking together (Fig. 4A and B). The second week saw a change in these aggregates into a radiating arrangement (Fig. 4C and D). After 5 weeks of mixing, the secondary minerals further changed into smaller single crystals with monoclinic features (see arrows in Fig. 4E and F).

The energy-dispersive X-ray analysis (EDXA) spectra showed a difference in REE composition for these secondary minerals compared with the untreated monazite (Fig. 5B–D). Ce and La were found to be the only REE in the secondary minerals at every growth stage. The presence of Nd and F, which were present in low amounts in the untreated monazite, was not detected in the newly formed biominerals. The 1-, 2- and 5-week samples all had a high O:C ratio and a similar relative abundance of Ce-La, which was similar to the untreated samples (Fig. 5B and D). However, the 3- and 4-week samples showed a low O:C ratio and large peaks for Ce and La (Fig. 5C). EDXA of the secondary minerals from the spent MCD liquid culture reaction showed a similar elemental composition to those resulting from the MCD plates except for larger peaks for Ce and La (Fig. 6).

Mineralogical examination of untreated monazite

EDXA showed that the Gakara monazite sample contained four lanthanides, i.e. cerium, lanthanum, neodymium and praseodymium (Fig. 5A). Barium was present as a non-REE metal in the sample. Other non-metallic elements were identified as carbon, fluorine, oxygen, phosphorus and sulphur. X-ray fluorescence (XRF) confirmed that the sample was composed of 22.7% Ce, 16.8% La, 5.9% Nd, 4.2% Ba and 1.3% Pr (Table 1). The monazite also contained a negligible array of other REE including samarium (Sm), gadolinium (Gd), thorium (Th) and yttrium (Y). X-ray diffraction (XRD) analysis (Fig. 7) revealed a match of the sample with the Joint Committee on Powder Diffraction Standards (JCPDS) mineral phases including $(La, Nd)_2(CO_3)_3{\cdot}8H_2O$, $CeCO_3F$, $LaCO_3F$, $La_7P_3O_{18}$, $LaPO_4$ and $CePO_4$.

XRD analysis of the secondary mycogenic biominerals

Biominerals of the first and final week's treatment were subjected to XRD analysis. It was revealed that the sample incubated for 1 week with *A. niger* on MCD agar shared similar mineral phases to the untreated control except for a generally lower peak intensity (Fig. 8b). In addition to the mineral phases in the substrate, weak

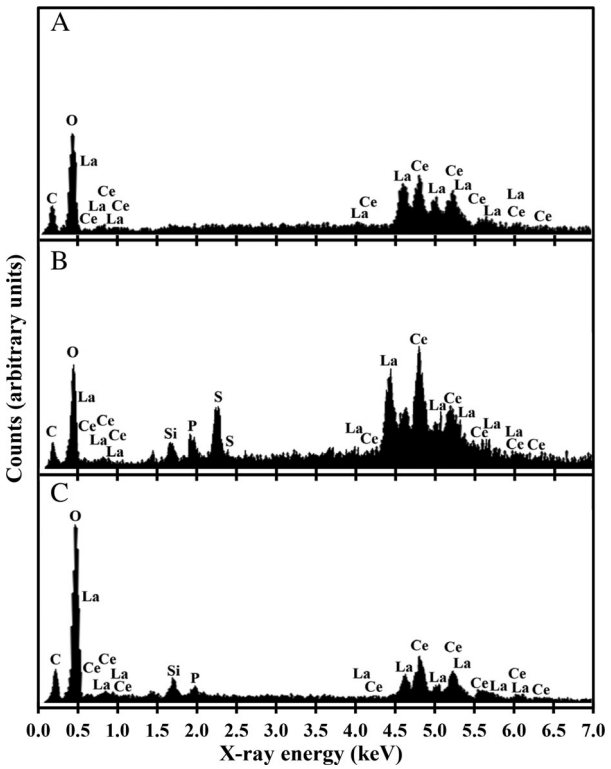

Fig. 6. Energy-dispersive X-ray analysis (EDXA) of the secondary biominerals after reaction of 1% (w/v) monazite and biomass-free *A. niger*-spent liquid MCD medium for (A) 1, (B) 2 and (C) 5 weeks at 25°C in the dark. The spent culture medium was obtained after 2 weeks of incubation at 25°C in the dark. Typical spectra are shown from several similar determinations.

peaks corresponding to Ce and La oxalates were observed in samples from the fifth week of incubation (Fig. 9b). In the interaction with spent liquid culture medium, the 1-week incubation sample also showed similar results to the control (Fig. 8a). Patterns linked to Ce and La oxalates of prominently higher intensity were observed in the 5-week sample (Fig. 9a).

Geochemical modelling

Solubility diagrams predicting the fate of lanthanide under three scenarios were constructed. The solubility constant chosen to input for lanthanide was $K_{sp} = 5.07 \times 10^{-26}$, which was determined by measuring the solubility of chemically precipitated cerium oxalate under laboratory conditions. The amount of oxalic acid in the simulation system was set at 55 mM, an actual oxalate concentration found in the liquid MCD medium after 2 weeks incubation with *A. niger* in preliminary experiments (Kang and Gadd, unpublished). The system of log $a[(C_2O_4)^{2-}]$ versus pH (Fig. 10A) showed the transformation of lanthanide as three insoluble minerals in the presence of different activities of oxalate over the full range of pH. The results

Table 1. Composition of the original Gakara monazite sample as determined using X-ray fluorescence.

Element[a]	Value (% by mass)
Ce	22.696
La	16.795
SiO_2	16.664
MnO	7.867
P_2O_5	6.855
Nd	5.931
F	4.595
Ba	4.243
Al_2O_3	3.885
Fe_2O_3	2.876
SO_3	2.828
Pr	1.330
CaO	1.001
Sm	0.707
K_2O	0.490
MgO	0.438
Gd	0.215
Sr	0.142
TiO_2	0.124
Th	0.092
Sn	0.082
Y	0.080
Zr	0.037
Cl	0.019
As	0.011

a. Some elements are expressed as oxides.

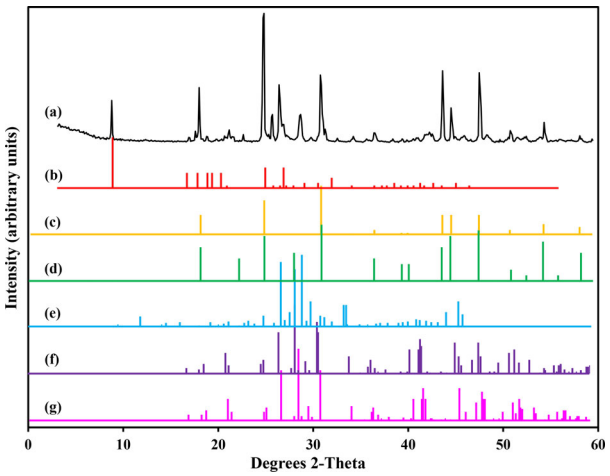

Fig. 7. (a) X-ray diffraction (XRD) pattern of the untreated Gakara monazite sample. Below are shown standard JCPDS card patterns: (b) no. 30-678, $(La, Nd)_2(CO_3)_3{\cdot}8H_2O$; (c) no. 11-340, $CeCO_3F$; (d) no. 41-595, $LaCO_3F$; (e) no. 33-719, $La_7P_3O_{18}$; (f) no. 32-493, $LaPO_4$; (g) no. 32-199, $CePO_4$. A typical pattern is shown from several similar determinations.

showed that at pH 0, the minimum concentration of oxalate required to form $Ln_2(C_2O_4)_3$ was $10^{-4.98}$ M. It was also revealed that Ln oxalate could be a possible mineral at a low pH and that higher amounts of oxalate would be required to precipitate Ln as the pH increased. Likewise, the system of log $a[(PO_4)^{3-}]$ versus pH (Fig. 10B) showed

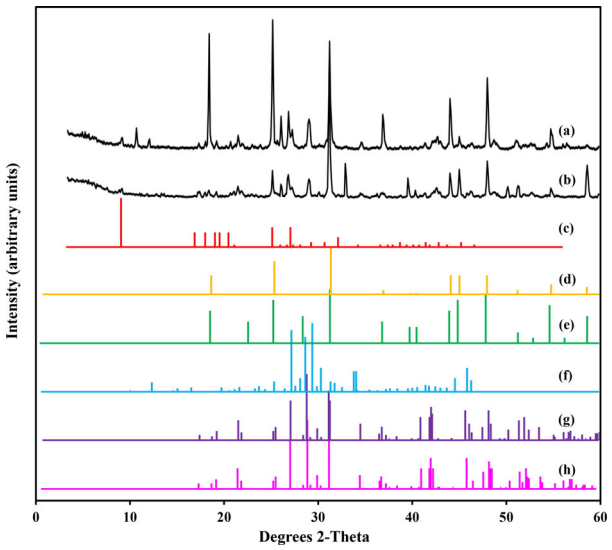

Fig. 8. (a) X-ray diffraction (XRD) pattern of the secondary biominerals after reaction of 1% (w/v) monazite and the *A. niger*-spent liquid MCD medium for 1 week. (b) Pattern of the secondary biominerals extracted from MCD agar containing 0.5% (w/v) monazite after 1-week growth of *A. niger* at 25°C in the dark. Below are shown standard JCPDS card patterns: (c) no. 30-678, (La, Nd)$_2$(CO$_3$)$_3$·8H$_2$O; (d) no. 11-340, CeCO$_3$F; (e) no. 41-595, LaCO$_3$F; (f) no. 33-719, La$_7$P$_3$O$_{18}$; (g) no. 32-493, LaPO$_4$; (h) no. 32-199, CePO$_4$. Typical patterns are shown from several similar determinations.

that in the presence of 55 mM oxalic acid and at acidic pH, Ln oxalate could occur at $a[(PO_4)^{3-}] < 10^{-19.91}$ M. Moreover, in order to precipitate Ln oxalate at a fixed pH of 1.59 and an undefined amount of phosphate and

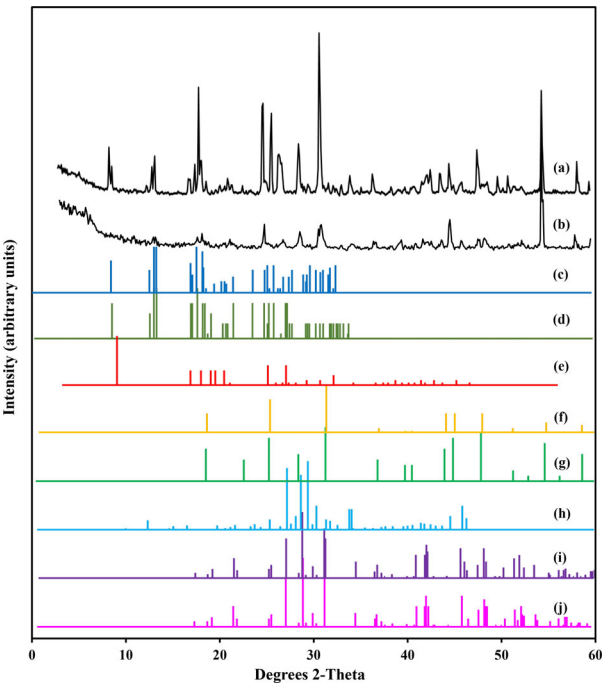

Fig. 9. (a) X-ray diffraction (XRD) pattern of the secondary biominerals after reaction of 1% (w/v) monazite and the *A. niger*-spent liquid MCD medium for 5 weeks. (b) Pattern of the secondary biominerals extracted from MCD agar containing 0.5% (w/v) monazite after the 5-week growth of *A. niger* at 25°C in the dark. Below are shown standard JCPDS card patterns: (c) no. 20-268, Ce$_2$(C$_2$O$_4$)$_3$·10H$_2$O; (d) no. 20-549, La$_2$(C$_2$O$_4$)$_3$·10H$_2$O; (e) no. 30-678, (La, Nd)$_2$(CO$_3$)$_3$·8H$_2$O; (f) no. 11-340, CeCO$_3$F; (g) no. 41-595, LaCO$_3$F; (h) no. 33-719, La$_7$P$_3$O$_{18}$; (i) no. 32-493, LaPO$_4$ and (j) no. 32-199, CePO$_4$. Typical patterns are shown from several similar determinations.

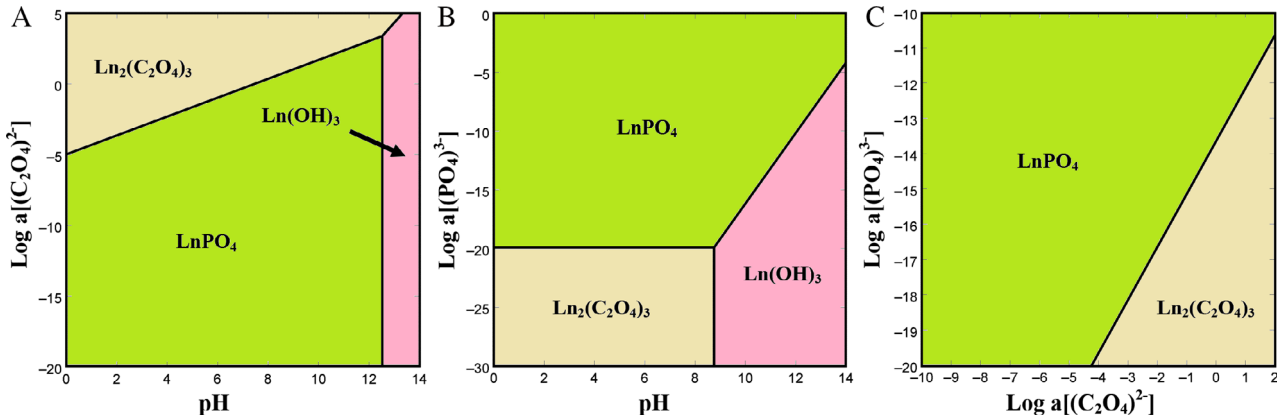

Fig. 10. Geochemical modelling of (A and C) lanthanide speciation in the monazite (LnPO$_4$)–*A. niger* interactions in solid MCD medium and (B) speciation in the interaction between monazite (LnPO$_4$) and biomass-free MCD medium after growth of *A. niger* for 2 weeks. The solubility diagrams simulate three conditions: (A) pH versus log $a[(C_2O_4)^{2-}]$ Ln speciation in the presence of oxalates at different pH values; (B) pH versus log $a[(PO_4)^{3-}]$ Ln speciation in the presence of phosphates at different pH values; (C) log $a[(C_2O_4)^{2-}]$ versus log $a[(PO_4)^{3-}]$: competitive speciation of Ln in the presence of oxalates and phosphates at pH 1.59. All the other chemical species were calculated according to their actual concentrations in the medium and included in the modelling systems at 25°C under 1.013 bar.

oxalate, an increase of phosphate must be matched by an increasing amount of oxalate (Fig. 10C).

Discussion

The Gakara REE deposit where the monazite sample originated is located in the East Africa Rift, which, in recent years, has been well known for supplying the rare earth industry (Lehmann *et al*., 1994). Geochronological data have shown that the REE veins in the area mainly consist of primary bastnaesite (REE-CO_3F) and monazite as secondary occurring minerals dating back to 602 and 589 Ma ago respectively (Ntiharirizwa *et al*., 2018). The presence of REE-carbonates was also confirmed by XRD in our work, which showed small amounts of $CeCO_3F$ and $LaCO_3F$. Our XRF results are in agreement with the elemental composition revealed in a survey of African monazite ores that found light REE in the following order of abundance: Ce > La > Nd > Pr (Harmer and Nex, 2016), and also showed that our monazite sample, as in other relevant studies on monazite, contains a slightly higher amount of Ce and La than other REE (Zhu and O'Nions, 1999; Galvin and Safarzadeh, 2018).

Fungal interactions with monazite have hitherto not been reported. The presented results from incubation of *A*. *niger* on solid medium suggest that the growth of the organism was retarded by the presence of monazite as the biomass showed a continuous decline with increasing amounts of monazite. The increase of surface pH on monazite-containing plates can probably be explained by the use of NO_3^- as the nitrogen source, buffering effects of the monazite, and lower acid production because of reduced growth. The general upward trend of biomass yield throughout the 5-week continuous incubation at a 0.5% monazite concentration indicated that *A*. *niger* could still grow at a lower rate. After 2 weeks of incubation, the surface pH showed a significant increase, which was the same as the pH trend in the liquid medium experiments. These results are consistent with recent work where similar pH shifts were observed during the bioleaching of laterite using *A*. *niger* grown in liquid media (Yang *et al*., 2019a). It is known that external medium pH can sometimes increase during incubation of *A*. *niger* on mineral-containing solid media and especially when nitrate is supplied as the inorganic nitrogen source (Sayer and Gadd, 1997; Ceci *et al*., 2015a; Ceci *et al*., 2015b). This has been commonly observed for fungal growth on nitrate because nitrate uptake in fungi occurs by NO_3^-/H^+ symport leading to alkalization of the external environment, while many fungi can also excrete NH_4^+, derived from NO_3^- metabolism, which also elevates the external pH (Zhou *et al*., 2000; Galvan and Fernández, 2001; Takasaki *et al*., 2004; Kramer-Haimovich *et al*., 2006; Stief *et al*., 2014; Watkinson *et al*., 2015).

Examination of the novel mycogenic biominerals revealed that, at each stage of fungal growth, the morphologies of the REE-containing secondary biominerals varied considerably. In solid media, at least four distinctive features for the crystals were observed including thin lamellar sheets, tabular plates, radiating needle clusters and rosette aggregates. Two additional morphologies involving tabular aggregates and individual monoclinic bodies were observed when monazite was incubated with biomass-free spent culture medium. These well-developed monoclinic or orthorhombic crystalline morphologies were observed in previous studies, which used calcite marble, Ca-phosphate rock and gypsum as the substrate for the precipitation of calcium by oxalic acid-producing fungi (Gharieb *et al*., 1998; Schneider *et al*., 2010; Sturm *et al*., 2015). However, there may be a variety of formation types for a given metal oxalate. For example, mycogenic calcium oxalate crystals can be categorized into four groups, i.e. tetragonal bipyramids, prisms, tablets and needles (Arnott, 1995). A difference in the mineral substrate, though containing the same metal, can also influence the size and shape of the secondary minerals produced. Fomina *et al.* (2005a) revealed that mycogenic lead oxalate precipitated by *Beauveria caledonica* exhibited tetragonal spikes in the presence of lead phosphate while irregular spikes occurred with lead tetraoxide, and octahedral bodies formed when lead carbonate was present. Mycogenic oxalates can also assume the form of orthorhombic tablets (glushinskite - magnesium oxalate), acicular clusters (strontium oxalate hydrate), rosettes and spheres (whewellite - calcium oxalate monohydrate and moolooite - copper oxalate hydrate) (Gadd, 2007), which were similar observations to our results. The only previous studies of lanthanides, to which our results could be comparable, are few and generally involve the transformation of a single element rather than multiple elements in a natural mineral substrate (Li and Gadd, 2017; Kang *et al*., 2019). Chemically synthesized Ce- or La-oxalate invariably take the form of plate-like single crystals and their sizes can vary from 10 to 300 μm in length depending on the precipitation method and concentrations of reagents (Claparede *et al*., 2011; Maslennikov *et al*., 2017; Yu *et al*., 2017). A rare case of flower-like aggregates of tabular crystals was reported for cerium oxalate decahydrate [$Ce_2(C_2O_4)_3{\cdot}10H_2O$] which were abiotically precipitated using pure oxalic acid (Liu *et al*., 2013). Few previous studies have paid attention to the mycogenic transformation of lanthanide elements. Large tabular-shaped crystals with a layered texture, which bore a resemblance to those in the present study, were formed as a result of the bioprecipitation of La oxalate in a solid medium containing lanthanum chloride (Kang *et al*., 2019). These crystals also showed prominent differences

in morphology from the lanthanum oxalate that was precipitated using liquid spent culture media (Kang *et al*., 2019).

The secondary minerals obtained in this study contained only Ce and La as REE and the only difference was in the relative proportion to C and O. The absence of other metals, including Nd, Pr and Ba, indicated these secondary minerals may be of high purity. XRD showed that, in both solid and liquid media, *A*. *niger* was able to transform monazite into Ce- and La-oxalates. The only difference was in the relative yield, which was clearly higher for the spent liquid culture medium as indicated by the higher peaks in the XRD patterns. The formation of oxalates in the liquid medium was accompanied by a sharp decrease in the total REE concentration after 3 weeks (Fig. 2). The excretion of organic acids, e.g. citric and oxalic acids can play a significant role in the dissolution of insoluble minerals and can be preceded by the formation of soluble metal–ligand complexes before oxalate-mediated precipitation occurs (Sayer and Gadd, 1997). Despite the involvement of organic acids, the bioleaching ability remained at a low level, which was in agreement with another study which found that other phosphate-solubilizing microbes showed quite a low efficiency in leaching Ce and La from monazite ores ranging from only 0.005% to 0.13% recovery (Shin *et al*., 2015) and also that direct rather than indirect contact may be essential for more efficient fungal bioleaching of elements from ores (Yang *et al*., 2019a).

Geochemical simulation is a useful method to investigate the transformation mechanisms for minerals and has been widely applied to different scenarios regarding fungal–mineral interactions (Ceci *et al*., 2015b; Li *et al*., 2019). Since the monazite contained a larger amount of Ce than La, our modelling systems were based on the solubility product of Ce-oxalate, which was measured under laboratory conditions. We did not carry out geochemical simulation for speciation of La-oxalate, which will produce very similar results to Ce because of its similar physicochemical properties and K_{sp} value. All three diagrams that were produced showed the possibility of oxalate transformation from phosphates. According to the modelling results, the possible mechanism through which Ln oxalates would be formed under these circumstances could be:

$$2LnPO_{4(aq)} + 9H_2O + 2H^+ + 3(C_2O_4)^{2-} \rightarrow Ln_2(C_2O_4)_3 \cdot 9H_2O_{(s)} + 2HPO_4^{2-} \quad (7)$$

Such a mechanism may be of importance to the biogeochemical cycling of REE because P-solubilizing fungi and bacteria are ubiquitous in soil environments (Jacobs *et al*., 2002; Fomina *et al*., 2004; Fomina *et al*., 2005b; Fomina *et al*., 2006). The solubilization of REE-bearing phosphate compounds also releases inorganic phosphate (P_i) and thus can improve soil fertility (Zhang *et al*., 2018). In a metallurgical process, REE-oxalate can be readily converted into REE-oxides through high-temperature treatment and therefore may also serve as a precursor for other useful REE materials (Kang *et al*., 2019). In conclusion, we have demonstrated the ability of *A*. *niger* to transform natural monazite into Ce- and La-containing crystalline oxalates $[Ln_x(C_2O_4^{2-})_y \cdot zH_2O]$ of distinct morphologies in solid media and also after interaction with biomass-free spent liquid culture medium, the latter method allowing Ln biorecovery in high purity. Our findings provide new knowledge on the interactions between REE and fungi, which also have potential application for the biorecovery of these strategically important elements from REE-containing solutions, process streams and leachates.

Experimental procedures

Microorganism, media and mineral

The microorganism used in our study was a wild-type strain of *A*. *niger* (ATCC 1015), which was routinely maintained on malt extract agar (MEA) (Lab M Limited, Bury, UK) in the dark at 25°C. Modified Czapek-Dox liquid medium (MCD) consisted of (l^{-1} Milli-Q water): sucrose 30 g, $NaNO_3$ 2 g, Na_2HPO_4 1 g, $MgSO_4 \cdot 7H_2O$ 0.5 g, KCl 0.5 g and $FeSO_4 \cdot 7H_2O$ 0.01 g. The final pH was adjusted to pH 5.5 with sterile 1 M HCl prior to autoclaving for 15 min at 115°C. For the preparation of solid media, 15 g of Agar No. 1 (Lab M Limited, Bury, UK) was added to 1 L of the liquid MCD medium. The medium was then autoclaved at 115°C for 15 min. The monazite concentrate, which was originally procured from the Gakara deposit, Burundi, East Africa, was kindly provided by Rainbow Rare Earths Limited (London, UK). The monazite was pulverized using a mortar and pestle, sieved through a 90-μm mesh and autoclaved for 15 min at 115°C before use.

Solid media experiments

Monazite-containing agar plates were made by incorporating 0.25%, 0.50%, and 1.0% (w/v) sterilized monazite powder into molten MCD agar medium when cooled to around 60°C. Cellophane membranes, which were used to separate mycelia from the agar, were prepared by autoclaving in Milli-Q water at 115°C for 15 min followed by washing three times in sterilized Milli-Q water. A sterile cellophane membrane (90 mm diameter) was placed on top of the agar surface and a plug (0.5 cm diameter), cut from a freshly grown *A*. *niger* colony using a sterile cork borer, was inoculated onto the centre of the plate. The

plates were incubated in the dark at 25°C for a total period of 5 weeks. Biomass was harvested and surface pH measured at weekly intervals at five points across the diameter of the agar plate using an Orion 3 Star benchtop pH meter (Thermo Fisher Scientific, Loughborough, UK) equipped with a flat-tip electrode (VWR International, Lutterworth, England, UK). Minerals were collected by gently homogenizing the agar in Milli-Q water at 80°C in a crystallizing dish after settling and washed at least three times with Milli-Q water. All solid media experiments were carried out at least in triplicate.

Liquid media experiments

Spore suspensions of *A. niger* were prepared by washing off spores from fully grown colonies on MEA using 0.1% (v/v) sterile TWEEN® 80 (Sigma-Aldrich, St Louis, MO, USA) and filtering through a sterile muslin cloth. *Aspergillus niger* spores were initially inoculated in 200 ml liquid MCD medium at 1×10^6 spores ml^{-1} in a 250 ml Erlenmeyer flask and shaken at 125 rpm for 2 weeks at 25°C in the dark. After this time, biomass-free spent medium was collected by vacuum filtration through 0.45 μm pore diameter cellulose acetate membrane filters (Whatman, Maidstone, UK). The reaction system contained 1.0% or 2.0% (w/v) monazite sand, which was achieved by adding sterilized monazite to 50 ml biomass-free medium in a 50 ml centrifuge tube. The tubes were mixed on a roller mixer for 1, 2, 3, 4 and 5 weeks at 25°C in the dark. Minerals were collected by centrifugation at 2553*g* for 30 min and washed with Milli-Q water at least three times. The supernatant pH was measured using the above-mentioned equipment. Measurements for total rare earth concentration in the liquid system after reaction were carried out using the Arsenazo III colorimetric method (Hogendoorn *et al*., 2018). This was achieved by mixing 1 ml of an appropriately diluted sample with 1 ml 0.02% (w/v) Arsenazo III solution (Sigma-Aldrich) and 8 ml pH 2.8 potassium hydrogen phthalate buffer. After the chromogenic reaction, the $OD_{658\ nm}$ of the mixture was measured using an Ultrospec 2100 pro spectrophotometer (Biochrom, Holliston, MA, USA).

EDXA, SEM, XRD and XRF

The elemental composition of the mineral samples was determined using EDXA. SEM was used to examine morphological features. XRD was used for determining mineral phases, and XRF was used for the measurement of elemental composition.

After collection, the mineral samples were dried in a desiccator for at least 1 week and mounted on adhesive carbon tape on $25 \times 5\ mm^2$ electron microscopy aluminium stubs (Agar Scientific, Essex, UK) before being examined using EDXA (Oxford Inca, Abingdon, Oxon, UK) operating at an accelerating voltage of 15 kV for 100 s. For SEM, samples on the stub were coated with a layer of 10 nm gold and platinum using a Cressington 208HR sputter coater (Ted Pella, Redding, CA, USA) prior to examination using a field emission scanning electron microscope (Jeol JSM7400F) operating at an accelerating voltage of 5 kV. Mineral phases were determined using a Hiltonbrooks X-ray diffractometer (XRD) (HiltonBrooks, Crewe, UK) furnished with a monochromatic CuKα source and curved graphite, single-crystal chronometer (30 mA, 40 kV). To prepare for XRD, samples were ground to a fine powder using a ceramic mortar and pestle and compacted tightly on the reverse side of an aluminium specimen holder ($15 \times 20 \times 2\ mm^3$) held against a glass slide. The back cover was then snapped into place and the glass slide was removed from the holder. Duplicate samples were analysed over the range 3–60° 2θ at a scan rate of $1°\ min^{-1}$ in 0.1° increments. To determine the elemental composition of the minerals, XRF spectroscopy was carried out using a Philips PW2424 sequential spectrometer with an RhKα source and calibrated with certified standard materials. The samples were placed in a 32-mm diameter pellet mould and were compacted under loads of 75 kN for 5 min and 150 kN for a further 10 min and then transferred to a specimen cup that had a 27-mm-diameter viewing aperture. The results are expressed as oxides.

Geochemical modelling

Geochemist's Workbench software, version 12.0.4 (Aqueous Solutions LLC, Champaign, USA) was used for simulating the geochemical fate of monazite in the fungal-mediated reaction systems. Three subprograms included in the software, i.e. Act2, SpecE8 and TEdit were also used for this purpose (Ceci *et al*., 2015a; Kang *et al*., 2019). To model the system in solid medium experiments, which contain a known amount of monazite ($LnPO_4$), the pH and concentration of oxalate were set as variables and a diagram of pH versus oxalate was created. To simulate the biomass-free supernatant reactions with monazite, in which pH and PO_4^{3-} were assumed to be the variables, a diagram of pH versus phosphate was constructed. In the case of a fixed pH in a solid medium, both PO_4^{3-} and oxalate were set as variables and a diagram of PO_4^{3-} versus oxalate was created. In these three scenarios, the molarities of all ions and anions were entered into the subprogram SpecE8 (the Visual MINTEQ database) as their actual concentrations in the MCD medium and the solubility diagrams were drawn using Act2. The activity of all the chemical species at 25°C and 1.013 bar was calculated using SpecE8 based on thermodynamic equilibria with the relationship

between activity and the concentration of aqueous species being expressed as:

$$a = \gamma[c] \quad (8)$$

where a is the activity, c is the actual concentration and γ is the activity coefficient ($c \rightarrow 0$, $\gamma = 1.0$ at infinite dilution). In the simulation systems, the activity of monazite ($LnPO_4$) was set as 1.0 because of its very low solubility. Since the database does not include the solubility product of hydrated Ce oxalate, a calculation was carried out according to the actual molarity of Ce ions in a saturated solution. For the determination of Ce^{3+} activity at equilibrium, Ce oxalate was completely precipitated by adding an excessive amount of oxalic acid into a 5 mM $CeCl_3$ solution. The resulting precipitate was washed multiple times with Milli-Q water and maintained on a roller mixer for 3 days until equilibrium was achieved. The actual concentration of Ce^{3+} in the supernatant of the saturated solution was measured using the Arsenazo III method at 25°C (Hogendoorn *et al*., 2018). The calculation was based on the equilibrium equation 6 and the following formula:

$$K_{sp}\left[Ce_2(C_2O_4)_3 \cdot xH_2O\right] = \left[a\left(Ce^{3+}\right)\right]^2 \times \left[a\left({C_2O_4}^{2-}\right)\right]^3 \quad (9)$$

where $a(Ce^{3+})$ and $a({C_2O_4}^{2-})$ represent the activities for Ce^{3+} and ${C_2O_4}^{2-}$ according to Eq. 7. The K_{sp} of $Ce_2(C_2O_4)_3{\cdot}xH_2O$ at 25°C was manually added into the database using the subprogram TEdit.

Statistical analysis

Data regarding biomass yield, REE concentration and pH were subjected to statistical analysis using IBM SPSS Statistics 22.0. Tukey's HSD post hoc test in one-way ANOVA was applied to compare the significance of difference at $P < 0.05$ between treatments. All data were from at least three replicates for each treatment.

Acknowledgements

G.M.G. gratefully thanks the Natural Environment Research Council (NE/M010910/1 (TeaSe); NE/M011275/1 (COG^3)) for financial support of the Geomicrobiology Group. X.K. gratefully acknowledges receipt of financial support through a China Scholarship Council - School of Life Sciences, University of Dundee PhD Scholarship (No. 201606910077). The authors' thanks are also due to Mr. Martin Eales, CEO of Rainbow Rare Earths (London, UK) for kindly donating the Gakara monazite sample. The authors also thank Dr. Yongchang Fan (Materials and Photonics Systems Group, University of Dundee) for assistance with scanning electron microscopy and energy-dispersive X-ray spectroscopy.

References

Arnott, H.J. (1995) Calcium oxalate in fungi. In *Calcium Oxalate in Biological Systems*, Khan, S.R. (ed). Boca Raton: CRC Press, pp. 73–111.

Barmettler, F., Castelberg, C., Fabbri, C., and Brandl, H. (2016) Microbial mobilization of rare earth elements (REE) from mineral solids - a mini review. *AIMS Microbiol* **2**: 190–204.

Brisson, V.L., Zhuang, W.-Q., and Alvarez-Cohen, L. (2016) Bioleaching of rare earth elements from monazite sand. *Biotechnol Bioeng* **113**: 339–348.

Ceci, A., Kierans, M., Hillier, S., Persiani, A.M., and Gadd, G.M. (2015a) Fungal bioweathering of mimetite and a general geomycological model for lead apatite mineral biotransformations. *Appl Environ Microbiol* **81**: 4955–4964.

Ceci, A., Rhee, Y.J., Kierans, M., Hillier, S., Pendlowski, H., Gray, N., *et al*. (2015b) Transformation of vanadinite [$Pb_5(VO_4)_3Cl$] by fungi. *Environ Microbiol* **17**: 2018–2034.

Chelgani, S.C., Rudolph, M., Leistner, T., Gutzmer, J., and Peuker, U.A. (2015) A review of rare earth minerals flotation: monazite and xenotime. *Int J Min Sci Technol* **25**: 877–883.

Chi, R., and Xu, Z. (1999) A solution chemistry approach to the study of rare earth element precipitation by oxalic acid. *Metall Mater Trans B* **30**: 189–195.

Claparede, L., Clavier, N., Dacheux, N., Moisy, P., Podor, R., and Ravaux, J. (2011) Influence of crystallization state and microstructure on the chemical durability of cerium-neodymium mixed oxides. *Inorg Chem* **50**: 9059–9072.

Deng, X., Chai, L., Yang, Z., Tang, C., Wang, Y., and Shi, Y. (2013) Bioleaching mechanism of heavy metals in the mixture of contaminated soil and slag by using indigenous *Penicillium chrysogenum* strain F1. *J Hazard Mater* **248**: 107–114.

Fomina, M., Bowen, A.D., Charnock, J.M., Podgorsky, V.S., and Gadd, G.M. (2017) Biogeochemical spatio-temporal transformation of copper in *Aspergillus niger* colonies grown on malachite with different inorganic nitrogen sources. *Environ Microbiol* **19**: 1310–1321.

Fomina, M., Charnock, J.M., Hillier, S., Alexander, I.J., and Gadd, G.M. (2006) Zinc phosphate transformations by the *Paxillus involutus*/pine ectomycorrhizal association. *Microb Ecol* **52**: 322–333.

Fomina, M., Hillier, S., Charnock, J.M., Melville, K., Alexander, I.J., and Gadd, G.M. (2005a) Role of oxalic acid overexcretion in transformations of toxic metal minerals by *Beauveria caledonica*. *Appl Environ Microbiol* **71**: 371–381.

Fomina, M.A., Alexander, I.J., Colpaert, J.V., and Gadd, G. M. (2005b) Solubilization of toxic metal minerals and metal tolerance of mycorrhizal fungi. *Soil Biol Biochem* **7**: 851–866.

Fomina, M.A., Alexander, I.J., Hillier, S., and Gadd, G.M. (2004) Zinc phosphate and pyromorphite solubilization by soil plant-symbiotic fungi. *Geomicrobiol J* **21**: 351–366.

Furrow, S.D., Cervellati, R., and Greco, E. (2012) A study of the cerium-catalyzed Briggs-Rauscher oscillating reaction. *Z Naturforsch B* **67**: 89–97.

Gadd, G.M. (2007) Geomycology: biogeochemical transformations of rocks, minerals, metals and radionuclides by fungi, bioweathering and bioremediation. *Mycol Res* **111**: 3–49.

Gadd, G.M. (2010) Metals, minerals and microbes: geomicrobiology and bioremediation. *Microbiol* **156**: 609–643.

Gadd, G.M., Bahri-Esfahani, J., Li, Q.W., Rhee, Y.J., Wei, Z., Fomina, M., and Liang, X.J. (2014) Oxalate production by fungi: significance in geomycology, biodeterioration and bioremediation. *Fungal Biol Rev* **28**: 36–55.

Galvan, A., and Fernández, E. (2001) Eukaryotic nitrate and nitrite transporters. *Cell Mol Life Sci* **58**: 225–233.

Galvin, J., and Safarzadeh, M.S. (2018) Decomposition of monazite concentrate in potassium hydroxide solution. *J Environ Chem Eng* **6**: 1353–1363.

Gharieb, M.M., Sayer, J.A., and Gadd, G.M. (1998) Solubilization of natural gypsum ($CaSO_4{\cdot}2H_2O$) and the formation of calcium oxalate by *Aspergillus niger* and *Serpula himantioides*. *Mycol Res* **102**: 825–830.

Goodenough, K.M., Schilling, J., Jonsson, E., Kalvig, P., Charles, N., and Tuduri, J. (2016) Europe's rare earth element resource potential: an overview of REE metallogenetic provinces and their geodynamic setting. *Ore Geol Rev* **72**: 838–856.

Harmer, R., and Nex, P. (2016) Rare earth deposits of Africa. *Episodes* **39**: 381–406.

Hassanien, W.A.G., Desouky, O.A.N., and Hussien, S.S.E. (2013) Bioleaching of some rare earth elements from Egyptian monazite using *Aspergillus ficuum* and *Pseudomonas aeruginosa*. *Walailak J Sci Technol* **11**: 809–823.

Hogendoorn, C., Roszczenko-Jasińska, P., Martinez-Gomez, N.C., de Graaff, J., Grassl, P., and Pol, A. (2018) A facile Arsenazo III based assay for monitoring rare earth element depletion from cultivation media of methanotrophic and methylotrophic bacteria. *Appl Environ Microbiol* **84**: e02887–e02817.

Humphries, M. (2012) *Rare Earth Elements: The Global Supply Chain*. Washington, DC: U.S. Congressional Research Service.

Jacobs, H., Boswell, G.P., Ritz, K., Davidson, F.A., and Gadd, G.M. (2002) Solubilization of metal phosphates by *Rhizoctonia solani*. *Mycol Res* **106**: 1468–1479.

Jernejc, K., Cimerman, A., and Perdih, A. (1982) Citric acid production in chemically defined media by *Aspergillus niger*. *Eur J Appl Microbiol Biotechnol* **14**: 29–33.

Kang, X., Csetenyi, L., and Gadd, G.M. (2019) Biotransformation of lanthanum by *Aspergillus niger*. *Appl Microbiol Biotechnol* **103**: 981–993.

Khanchi, A.R., Sedighi, H., Ansar, S., and Fasihi, J. (2014) Preconcentration of rare earth elements from Iranian monazite ore by spiral separator using multi-response optimization method. *Int J Min Sci Technol* **24**: 117–121.

Kramer-Haimovich, H., Servi, E., Katan, T., Rollins, J., Okon, Y., and Prusky, D. (2006) Effect of ammonia production by *Colletotrichum gloeosporioides* on pelB activation, pectate lyase secretion, and fruit pathogenicity. *Appl Environ Microbiol* **72**: 1034–1039.

Kumari, A., Panda, R., Jha, M.K., Kumar, J.R., and Lee, J.Y. (2015) Process development to recover rare earth metals from monazite mineral: a review. *Miner Eng* **79**: 102–115.

Lehmann, B., Nakai, S.I., Höhndorf, A., Brinckmann, J., Dulski, P., Hein, U.F., and Masuda, A. (1994) REE mineralization at Gakara, Burundi: evidence for anomalous upper mantle in the western Rift Valley. *Geochim Cosmochim Acta* **58**: 985–992.

Li, Q., and Gadd, G.M. (2017) Fungal nanoscale metal carbonates and production of electrochemical materials. *J Microbial Biotechnol* **10**: 1131–1136.

Li, Q., Liu, D., Chen, C., Shao, Z., Wang, H., and Liu, J. (2019) Experimental and geochemical simulation of nickel carbonate mineral precipitation by carbonate-laden ureolytic fungal culture supernatants. *Environ Sci - Nano* **6**: 1866–1875.

Li, Q., Csetenyi, L., and Gadd, G.M. (2014) Biomineralization of metal carbonates by *Neurospora crassa*. *Environ Sci Technol* **48**: 14409–14416.

Liang, X., and Gadd, G.M. (2017) Metal and metalloid biorecovery using fungi. *J Microbial Biotechnol* **10**: 1199–1205.

Liang, X., Kierans, M., Ceci, A., Hillier, S., and Gadd, G.M. (2016) Phosphatase-mediated bioprecipitation of lead by soil fungi. *Environ Microbiol* **18**: 219–231.

Liu, W., Feng, L., Zhang, C., Yang, H., Guo, J., and Liu, X. (2013) A facile hydrothermal synthesis of 3D flowerlike CeO_2 via a cerium oxalate precursor. *J Mater Chem A* **1**: 6942–6948.

Maslennikov, D.V., Matvienko, A.A., Sidelnikov, A.A., and Chizhik, S.A. (2017) A study of the effect of structural transformations in the course of $Ce_2(C_2O_4)_3{\cdot}10H_2O$ thermal decomposition on the morphology of CeO_2 obtained. *Mater Today* **4**: 11495–11499.

Massari, S., and Ruberti, M. (2013) Rare earth elements as critical raw materials: focus on international markets and future strategies. *Resour Policy* **38**: 36–43.

Moss, R.L., Tzimas, E., Willis, P., Arendorf, J., Thompson, P., and Chapman, A. (2013) Critical metals in the path towards the decarbonisation of the EU energy sector. Assessing rare metals as supply-chain bottlenecks in low-carbon energy technologies. Joint Research Centre Report EUR 25994.

Moustafa, M.I., and Abdelfattah, N.A. (2010) Physical and chemical beneficiation of the Egyptian beach monazite. *Resour Geol* **60**: 288–299.

Ng, D.H.P., Kumar, A., and Cao, B. (2016) Microorganisms meet solid minerals: interactions and biotechnological applications. *Appl Microbiol Biotechnol* **100**: 6935–6946.

Ntiharirizwa, S., Boulvais, P., Poujol, M., Branquet, Y., Morelli, C., Ntungwanayo, J., and Midende, G. (2018) Geology and U-Th-Pb dating of the Gakara REE deposit, Burundi. *Minerals* **8**: 394.

Panda, R., Kumari, A., Jha, M.K., Hait, J., Kumar, V., Rajesh Kumar, J., and Lee, J.Y. (2014) Leaching of rare earth metals (REMs) from Korean monazite concentrate. *J Ind Eng Chem* **20**: 2035–2042.

Rawlings, D.E., Dew, D., and du Plessis, C. (2003) Biomineralization of metal-containing ores and concentrates. *Trends Biotechnol* **21**: 38–44.

Reed, D.W., Fujita, Y., Daubaras, D.L., Jiao, Y., and Thompson, V.S. (2016) Bioleaching of rare earth elements

from waste phosphors and cracking catalysts. *Hydrometallurgy* **166**: 34–40.

Sayer, J.A., and Gadd, G.M. (1997) Solubilization and transformation of insoluble inorganic metal compounds to insoluble metal oxalates by *Aspergillus nger*. *Mycol Res* **101**: 653–661.

Schneider, K., Van Straaten, P., De Orduña, R.M., Glasauer, S., Trevors, J., Fallow, D., and Smith, P. (2010) Comparing phosphorus mobilization strategies using *Aspergillus niger* for the mineral dissolution of three phosphate rocks. *J Appl Microbiol* **108**: 366–374.

Shin, D., Kim, J., Kim, B.-S., Jeong, J., and Lee, J.-C. (2015) Use of phosphate solubilizing bacteria to leach rare earth elements from monazite-bearing ore. *Minerals* **5**: 189–202.

Stief, P., Fuchs-Ocklenburg, S., Kamp, A., Manohar, C.-S., Houbraken, J., Boekhout, T., *et al*. (2014) Dissimilatory nitrate reduction by *Aspergillus terreus* isolated from the seasonal oxygen minimum zone in the Arabian Sea. *BMC Microbiol* **14**: 35.

Sturm, E.V., Frank-Kamenetskaya, O., Vlasov, D., Zelenskaya, M., Sazanova, K., Rusakov, A., and Kniep, R. (2015) Crystallization of calcium oxalate hydrates by interaction of calcite marble with fungus *Aspergillus niger*. *Am Mineral* **100**: 2559–2565.

Takasaki, K., Shoun, H., Yamaguchi, M., Takeo, K., Nakamura, A., Hoshino, T., and Takaya, N. (2004) Fungal ammonia fermentation, a novel metabolic mechanism that couples the dissimilatory and assimilatory pathways of both nitrate and ethanol. *J Biol Chem* **279**: 12414–12420.

Watkinson, S.C., Boddy, L., and Money, N.P. (2015) *The Fungi*, 3rd ed. London: Academic Press.

Yang, Y., Song, W., Ferrier, J., Liu, F., Csetenyi, L., and Gadd, G.M. (2019a) Biorecovery of cobalt and nickel using biomass-free culture supernatants from *Aspergillus niger*. *Appl Microbiol Biotechnol* **104**: 417–425.

Yang, Y., Ferrier, J., Csetenyi, L., and Gadd, G.M. (2019b) Direct and indirect bioleaching of cobalt from low grade laterite and pyritic ores by *Aspergillus niger*. *Geomicrobiol J* **36**: 940–949.

Yu, J.-B., Yang, Z.-G., Wang, Z.-H., Tu, T.-S., Zhang, Z.-Q., and Li, J.-Y. (2017) Synthesis of cerium oxalate hydrate by precipitation technique under external magnetic field. *Rare Met* **36**: 1–8.

Zhang, Y., Chen, F.-S., Wu, X.-Q., Luan, F.-G., Zhang, L.-P., and Fang, X.-M. (2018) Isolation and characterization of two phosphate-solubilizing fungi from rhizosphere soil of moso bamboo and their functional capacities when exposed to different phosphorus sources and pH environments. *PLoS One* **13**: e0199625.

Zhenghua, W., Xiaorong, W., Yufeng, Z., Lemei, D., and Yijun, C. (2001) Effects of apatite and calcium oxyphosphate on speciation and bioavailability of exogenous rare earth elements in the soil-plant system. *Chem Spec Bioavailab* **13**: 49–56.

Zhou, J.-J., Trueman, L.J., Boorer, K.J., Theodoulou, F.L., Forde, B.G., and Miller, A.J. (2000) A high affinity fungal nitrate carrier with two transport mechanisms. *J Biol Chem* **275**: 39894–39899.

Zhu, X., and O'Nions, R. (1999) Monazite chemical composition: some implications for monazite geochronology. *Contrib Mineral Petrol* **137**: 351–363.

Zhuang, W.-Q., Fitts, J.P., Ajo-Franklin, C.M., Maes, S., Alvarez-Cohen, L., and Hennebel, T. (2015) Recovery of critical metals using biometallurgy. *Curr Opin Biotechnol* **33**: 327–335.